
Article:
Fan, Y., Zhang, L.X., Li, K. et al. (Accepted: 2026) Attention-BiLSTM for Timely Detection and Adaptive Classification of EMI and IEMI in 5G-Railways Wireless Communications. IEEE Transactions on Intelligent Transportation Systems. ISSN: 1524-9050 (In Press)

Attention-BiLSTM for Timely Detection and Adaptive Classification of EMI and IEMI in 5G-Railways Wireless Communications

Yejing Fan, *Student Member, IEEE,* Li Zhang, *Senior Member, IEEE,* Kang Li, *Senior Member, IEEE,* Mi Yang, *Member, IEEE,* Xuejian Zhang, *Student Member, IEEE,* Ruisi He, *Senior Member, IEEE* Mowei Lu, *Student Member, IEEE*

***Abstract*—High reliability and low latency are essential to railway wireless communications, which transmit train control and dispatch commands to ensure operational safety. However, as railway systems become increasingly electrified and more complex, the exposure to electromagnetic interference (EMI) also grows, potentially causing service disruptions and compromising safety. Intentional EMI (IEMI), which is deliberately and often maliciously generated, further increases the vulnerability of these critical communication networks. Real-time detection and classification of EMI and IEMI therefore become increasingly important. This paper presents composite models that reflect realistic railway scenarios and proposes an adaptive classification approach for EMI and IEMI using a deep learning algorithm based on bidirectional long-short-term memory (BiLSTM) networks and attention mechanisms. By employing time-series feature extraction to analyze both time and frequency information at fine resolution, the proposed method demonstrates a classification accuracy of 94.98%. Simulation results outperform existing techniques with a 3% improvement in accuracy, showcasing its adaptability across four typical railway scenarios at train speeds of up to 500 km/h. Moreover, online monitoring phase performs real-time detection in just 7.43 ms, meeting the stringent latency requirements for railway systems. Validation using real-world data further confirms the practical applicability of the proposed methods under actual operating conditions.**

***Index Terms*—Electromagnetic interference (EMI), Intentional EMI (IEMI), Deep Learning Algorithm, Detection, Classification, Railway Wireless Communications, 5G-Railway (5G-R)**

I. Introduction

THE railway transportation system is widely recognized as an economical, effective, and environmentally friendly mode of transporting goods and passengers [1]. Future intelligent railway wireless communication systems require reliable transmission, high data rates, and low latency for key services and passenger safety, even at speeds up to 500 km/h [2], [3]. With the commercialization of 5G, applying 5G to railway systems (5G-R) has garnered substantial interest. In Europe, the International Union of Railways (UIC) has introduced the Future Railway Mobile Communication System (FRMCS) through initiatives such as 5GRAIL [4], which supports digitized and automated services in line with reliability, availability, maintenance, and safety (RAMS) standards as the successor to GSM-R. China is directly transitioning from GSM-R to 5G-R, bypassing LTE-R [5]. Therefore, ensuring the safety and reliability of private 5G-R communication systems is critical for future intelligent railway operations.

The growing complexity of electrified railway systems has increased the vulnerability of wireless transmissions to electromagnetic interference (EMI) [6]. EMI can originate from natural events or onboard train equipment, such as lightning strikes, pantograph-catenary arcing, relays, and electric motors. Intentional EMI (IEMI), or jamming, involves malicious wireless signals deliberately introduced to disrupt wireless networks [7]. The increasing availability of compact communication devices further elevates risks associated with terrorism and criminal activities [8], [9]. In dense 5G deployments, additional base stations (BSs) and user equipment exacerbate interference, degrading signal quality, triggering signal processing malfunctions, and ultimately affecting automatic train protection [10], [11]. Even short outages can force trains to safety mode, causing emergency brakes, congestion, or accidents. Given that Railway wireless communications carries critical train control information, there is minimal tolerance for EMI compared to public networks. Hence, timely detection and classification of EMI and IEMI are vital for operational safety.

Accurate, low-latency classification further enables precise mitigation and resilience strategies [12]. Transient EMI, such as pantograph–catenary arcing, can be suppressed through transient blanking and forward-error correction; systematic logging of these events supports proactive maintenance by revealing arcing hotspots and early equipment wear. External EMI originating from neighbouring 5G base stations or public networks is best alleviated through dedicated network planning and real-time interference coordination that reallocates carriers or adapts transmit power. By contrast, IEMI constitutes a cyber-physical threat: rapid discrimination from unintentional EMI allows immediate activation of adaptive power-control or frequency-hopping defences, ensuring the 10 ms safety window required for signalling, traction-control,

Yejing Fan, Li Zhang, and Kang Li are with the School of Electronic and Electrical Engineering, University of Leeds, Leeds, UK (e-mail: el17yf@leeds.ac.uk; L.X.Zhang@leeds.ac.uk; K.Li1@leeds.ac.uk).
Mi Yang, Xuejian Zhang, and Ruisi He are with the School of Electronics and Information Engineering, Beijing Jiaotong University, Beijing 100044, China (e-mail: myang@bjtu.edu.cn; 23115029@bjtu.edu.cn; ruisi.he@bjtu.edu.cn).
Mowei Lu is with the Department of Engineering, University of Cambridge, Cambridge, U.K (e-mail: ml2010@cam.ac.uk).

and Communications-Based Train Control (CBTC)/ European Train Control System (ETCS) services [13].

Despite growing interest, current EMI detection research still faces limitations. Classical GSM-R detectors rely on fixed thresholds or simple statistics [9], [14] and struggle with dynamic 5G-R channels. Recent machine-learning approaches, Support Vector Machine (SVM), Random Forest (RF), and Agglomerative Hierarchical Clustering (AHC) [9], [15], [16], focus mainly on frequency-domain features for spectrum analysis. Railway wireless communications exhibits unique characteristics, including track-aligned coverage and predictable train trajectories. These can reveal patterns suitable for time-series data analysis and deep learning methods. In addition, modelling EMI/IEMI across diverse environments, cuttings, viaducts, and platforms remains challenging, especially under high-mobility 5G-R scenarios [17]. These gaps motivate the adaptive and time-series-based classification framework proposed in this paper.

This paper investigates time-series detection and classification using attention mechanisms and Long Short-Term Memory (LSTM). Compared to other deep learning and traditional machine learning methods, LSTM excels in capturing long-term dependencies and temporal patterns in sequential data [18], [19]. The attention mechanism enhances this capability by focusing dynamically on the most relevant time steps, improving the interpretability and performance of the model [20]–[22]. Together, these techniques allow for more accurate and efficient processing of complex temporal data [23]–[26], especially in scenarios involving high mobility. In this research, a variety of simulated EMI and IEMI signals are generated and superimposed to form a comprehensive signal sample space, from which the signal characteristics in specific train-operation intervals can be learned. Because train trajectories are fixed and the radio environment around the track is relatively stable, interference in 5G railway dedicated wireless systems exhibits certain regularity. By combining training data collected under different scenarios and train speeds, a "dynamic interference model" can be established. This model can be indexed by track segment (e.g., through a Geographic Information System (GIS)-based track database) to predict which type of interference is likely to appear on a given section and to support proactive mitigation strategies. Additionally, real-world data are collected through complex fading channels from a 5G-R test line to evaluate the proposed method. The main contributions of this paper are summarized below:

- The system model is built for various railway scenarios, considering realistic channel conditions. Five typical classes of EMI and IEMI are analyzed in detail.
- In the data pre-processing stage, a novel approach is introduced, extracting features from both real and imaginary components of the complex signals. This simultaneously captures detailed information from the time and frequency domains with enhanced resolution, preserving the critical signal characteristics necessary for accurate interference classification.
- A tailored Attention-BiLSTM deep learning architecture is proposed to classify EMI and IEMI under diverse railway scenarios and operational speeds. The stacked BiLSTM layers, combined with a self-attention mechanism, effectively capture temporal dynamics and emphasize critical signal segments.
- The proposed model is evaluated through simulations, achieving real-time detection in 7.43 ms with an accuracy of 94.98%, surpassing existing state-of-the-art methods by approximately 3%. The model showcases strong adaptability across four typical railway scenarios at train speeds up to 500 km/h.
- The practical applicability of the proposed methods is further validated using real-world measurement data collected from 5G-R test facilities. Results maintains an accuracy of 92.5%, confirming the reliability and robustness of the method in realistic conditions and underscoring its potential for practical deployment in next-generation intelligent railway wireless communication networks.

The rest of the paper is organized as follows. Section II provides an overview of the system model and the process of feature extraction. Section III introduces the theoretical basis of LSTM and the attention mechanism and presents a detailed structure of the Attention-BiLSTM-based classification algorithm. The simulation results and analysis are given in Section IV, followed by real data validation and discussions in Section V. The conclusion is drawn in Section VI.

II. System Model and Feature Extraction

A. Radio-Propagation Model and Representative Scenarios

The railway wireless communication system considered in this study, as shown in Fig. 1, consists of a 5G-R BS operating at 2.16 GHz, transmitting signals to a train antenna receiver mounted on the train roof. The chosen frequency band aligns with the 5G-R private network communication system tested in China in September 2023, utilizing the downlink 2155-2165 MHz frequency band [27]. Fig. 1 illustrates potential interferences, including transient EMI from pantograph-catenary arcing and IEMI at two different locations: originating from a portable device in a passenger's pocket within the train and originating from a power source placed on the ground between the BSs. Four main and representative scenarios are selected from the 18 communication scenarios [28], enabling a comprehensive evaluation of a complex railway environment.

We employ the 5G-R dynamic propagation model previously validated in our conference paper [7], which combines a Rician fading channel, log-distance path-loss, and Doppler shift. The received power is

$$P_r = A_1\sqrt{\tfrac{K}{K+1}}\big(P_t - PL(d_1)\big) + \sum_{i=2}^{N} A_i\sqrt{\tfrac{1}{K+1}}\big(P_t - PL(d_i)\big), \tag{1}$$

with path loss $PL(d) = PL(d_0) + 10\,n\log_{10}\big(d/d_0\big)$ and Doppler frequency $f_d = \frac{v\cdot f_c}{c}\cos\theta$. Full derivations and parameter-fitting details can be found in [7].

B. EMI and IEMI Classification

In this paper, five classes of EMI and IEMI in railway are investigated: (1) transient EMI, (2) frequency sweep IEMI

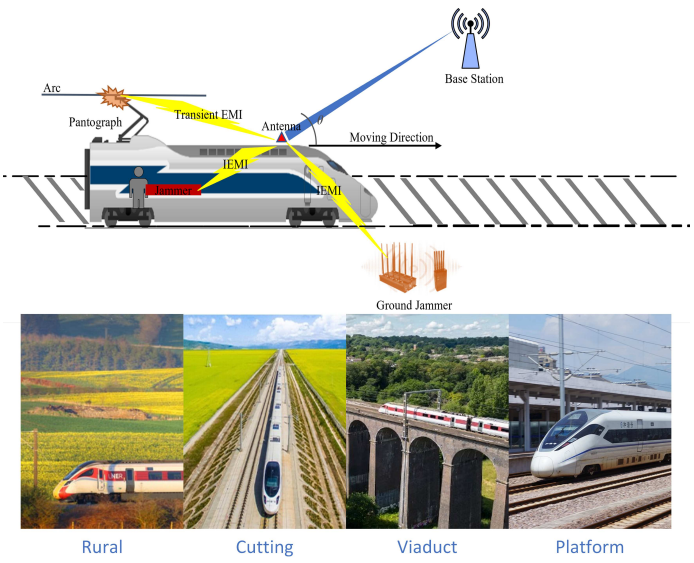

Fig. 1. The system model in railway wireless communication networks with various scenarios

on board, (3) frequency sweep IEMI on the ground, (4) synthesized frequency IEMI on board, and (5) synthesized frequency IEMI on the ground. These classes include typical transient EMI found in high-speed rail, as well as two types of frequency variation IEMI, each categorized by their locations, onboard the train or on the ground. A detailed discussion on the characteristics and impacts of EMI and IEMI on the electrified railway radio communication network can be found in the review paper [10].

Depending on the location of the IEMI, its impact can vary. The system model considers two cases: when the IEMI device is inside the train or on the ground. In the first scenario, the IEMI device is assumed to be portable, such as a jammer hidden in a passenger's pocket, typically with limited power capability (e.g., 1 W or +30 dBm) [29]. In the second case, the IEMI device is placed on the ground, where it is less constrained by size and power supply, often resulting in higher output power [30].

In the case of onboard IEMI generation, the coupling between the jammer and the antenna on the roof of the train remains relatively stable. The interference poses a significant threat to onboard wireless communication systems due to their proximity and minimal shielding between the interference source and the victim systems. The coupling loss between the jammer and the train antenna can be evaluated using the Friis transmission equation:

$$P_r = P_t \left(\frac{G_t G_r \lambda^2}{(4\pi)^2 R^2} \right) \tag{2}$$

where P_r is the received power at the antenna, P_t is the transmitted power, G_t and G_r are the gains of the transmitting and receiving antenna, λ is the wavelength of the signal, and R is the distance between the jammer and the antenna. The additional attenuation of the signal can be approximately 20 dB due to the effectiveness of the train structure shielding in the measurement [29]. Therefore, the total estimated coupling loss is determined by combining the free-space loss and attenuation due to obstructions, such as seats, passengers, and equipment.

In the second scenario, where the IEMI device is on the ground, refers to interference transmitted from a fixed position outside the train, targeting onboard communication systems as the train passes by. The power received at the antenna is primarily influenced by the train's movement. Considering the Doppler effect due to train movement, the frequency for each component can also be modeled, where $\theta(t)$ is the time-dependent angle between the direction of motion and the line connecting the train and the ground-based IEMI device. To effectively disrupt the communication signal, the ground-based jammer is strategically positioned to minimize obstacles, ensuring an optimal Line-of-Sight (LOS) to the train antenna. This scenario is evaluated using the two-ray LOS path loss model [29].

$$P_r = P_t \frac{G_t G_r h_t^2 h_r^2}{d^4} \tag{3}$$

where P_r is the received power at the train antenna, P_t is the transmitted power from jammer, G_t and G_r are the gains of the transmitting and receiving antenna, h_t and h_r are the heights of the transmitting and receiving antenna, and d is the distance between the jammer and the train antenna. The two-ray LOS path loss model assumes $d \gg h_t, h_r$, making it suitable for ground-to-train communication scenarios. Typical heights of railway antennas, approximately $h_t, h_r \approx$ 1-2 m for the train and the jammer, are significantly lower compared to the distances involved in most cases. The location of the jammer can vary significantly, such as being located near the BS, between multiple BSs, or within the train station, causing notable fluctuations in the power received at the train antenna. Even when the jammer is positioned as close as 10 meters from the train antenna, such as directly along the railway track or on a station platform, the model remains applicable and the jammer can substantially degrade the useful signal [29]. In this case, the total coupling loss includes contributions from both the Doppler shift and the two-ray LOS path loss.

C. Time-Frequency analysis of EMI and IEMI

The Short-Time Fourier Transform (STFT) is employed to calculate these short-term frequency variations by segmenting the signal into smaller time windows and analyzing the frequency content of each segment. In signal analysis, there is an inherent trade-off between time and frequency resolution due to the Heisenberg uncertainty principle [31]. A shorter window length provides better time resolution, enabling the capture of transient features more precisely. However, it reduces frequency resolution, making it challenging to distinguish closely spaced frequency components. Conversely, a longer window improves frequency resolution but at the expense of time resolution, potentially smearing out transient EMI. Balancing these resolutions is crucial for accurately capturing the transient effects of interference while maintaining sufficient frequency resolution to detect frequency variations of IEMI. Therefore, we need to strike a trade-off between fine time resolution and fine frequency resolution, as they cannot be

optimized simultaneously. For the STFT analysis, we use a small window length of 80 samples, which, given a sampling frequency of 20 MHz (sampling period T_s = 50 ns), provides a time resolution of:

$$\text{Window Duration} = \text{Window Length} \times T_s = 80 \times 50\,\text{ns} = 4\ \mu\text{s}.$$

A 4 μs window offers high time resolution to capture short transient EMI bursts (on the average of 5 μs repetition periods observed in measurements). An overlap of 25% (20 samples) is applied to ensure a smooth transition between consecutive windows to prevent missing transient events that may occur at the window edges. Overlapping windows helps in capturing transient EMI more effectively by providing more temporal data points for analysis. To enhance frequency resolution without sacrificing time resolution, we increase the number of FFT points (nfft) used in the STFT. Specifically, we set $nfft = 1024$ points. With a sampling frequency of 20 MHz, this results in a frequency resolution of

$$\Delta f = \frac{F_s}{\text{nfft}} = \frac{20\,\text{MHz}}{1024} \approx 19.5\,\text{kHz}.$$

This means that the frequency axis of the STFT will have bins spaced approximately 19.5 kHz apart, allowing the detection of fine frequency variations in the signal (e.g., certain frequency-sweep interference sweep a 10 MHz band within 50 μs, which requires high spectral resolution to distinguish). By zero-padding the windowed signal to the desired nfft length before computing the FFT, we achieve higher frequency resolution without altering the actual time resolution determined by the window length. Zero-padding interpolates the frequency spectrum, providing a smoother and more detailed frequency representation.

These STFT parameters, including the window length, overlap, and nfft, were selected through extensive trials and empirical testing, considering computational cost constraints [32], [33]. The comprehensive time-frequency representation of the entire signal sequence is obtained, offering detailed insights into the characteristics of both the time and frequency domain.

D. EMI and IEMI Model

a) Transient EMI: Transient EMI refers to short-duration EM disturbances in the radio frequency spectrum, which can be caused by various sources during train operation, including pantograph-catenary arcing, electronic equipment on board, lightning strikes, power surges, or other electromagnetic events [34]. In this paper, the typical transient EMI observed as a sparking or arcing, which often occurs between the catenary and the pantograph in the high-speed rail system, is analyzed. Transient EMI can be effectively modeled using damped sinusoidal signal characteristics.

$$V_{trans(t)} = A\left(e^{\frac{-t}{t_{rise}}} - e^{\frac{-t}{t_{hold}}}\right) \cdot sin(2\pi f_c t) \cdot \mu(t) \qquad (4)$$

where A is amplitude, t_{rise} is rise time, t_{hold} is duration, and f_c is the center frequency of the superimposed useful signal. The two consecutive transient interferences are separated by a similar amplitude 1 V, rise time 1 ns, and duration 20 ns based on measurements [35]. The repetition rate, defined as the interval between two consecutive transient interferences has an average 5 μs, but increase due to operating conditions such as the train's high speed, the contact surfaces of the pantograph and catenary degradation, and adverse weather conditions.

In the time domain, the transient EMI signal exhibits a short-duration characteristic, appearing as a brief burst of interference. In the frequency domain, the transient EMI signal exhibits a broad spectrum that extends beyond the typical useful signal bandwidth, covering a wide range of frequencies. This broad spectrum characteristic significantly overlaps with the useful signal, undermining the effectiveness of traditional mitigation methods such as frequency-hopping spread spectrum, which rely on sporadically changing the carrier frequency to avoid narrowband interferences and thus become ineffective against wideband interference. Furthermore, transient EMI has a variable repetition rate, making its behavior more unpredictable, similar to a random jammer that alternates between active and idle states, further complicating its detection and mitigation in railway communication systems [15]. Using STFT, the time-frequency representation of the transient EMI on 100 μs is shown in Fig. 2. Detection and classification of transient interferences can guide proactive maintenance efforts by identifying early signs of equipment degradation, such as pantograph-catenary interface wear. Addressing these issues promptly improves equipment health, thereby enhancing the reliability and safety of wireless railway communications.

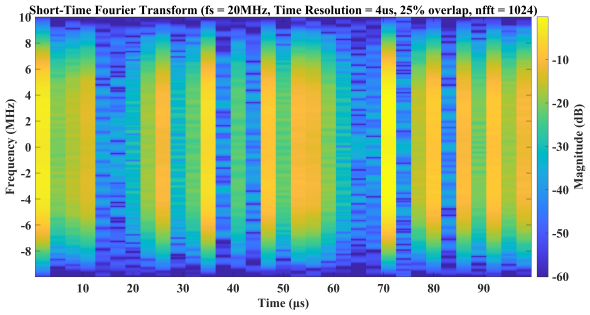

Fig. 2. Time-frequency representation of the transient EMI

b) Frequency sweeping IEMI: Due to hardware constraints, such as the need for a high sampling rate in the analog-to-digital converter (ADC) and a broadband power amplifier, low-cost IEMI devices often cannot effectively attack multiple channels simultaneously. As a result, frequency-sweeping IEMI is more commonly used [11].

Frequency sweep IEMI can be modeled by transmitting a continuous high-power noise sweep from one channel to another following a fixed strategy and repeating this process over time [35].

$$s(t) = Acos\left(2\pi\left(\frac{f_2 - f_1}{2T} \times t + f_1\right) \times t\right),\ 0 < t < T \qquad (5)$$

where a cosine wave with amplitude A sweeps over a frequency band $[f1, f2]$ over a period of time T [6]. This type of jamming signal is intentionally designed to disrupt 5G-R

communications with a central frequency of 2.16 GHz and a bandwidth of 10 MHz. The signal sweeps frequencies in the range [2155,2165] MHz over a period of 50 μs. Fig. 3 shows the time-frequency representation of the frequency-sweeping IEMI signal obtained using STFT within a detection window of 500 μs. The STFT reveals a symmetrical pattern in the time-frequency domain, showcasing both positive and negative frequency components due to the signal's real-valued nature.

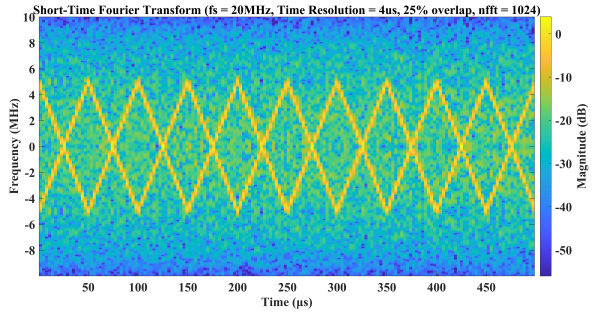

Fig. 3. Time-frequency representation of the onboard frequency sweeping IEMI

c) Frequency synthesized IEMI: Frequency-synthesized IEMI involves the simultaneous transmission of multiple interference signals at different frequencies, which can be fixed or dynamically changed. The synthesized interference is designed to mimic legitimate signals or exploit specific vulnerabilities in the communication system. To model synthesized frequency IEMI, the interference signal is represented as a sum of multiple sinusoidal components, each representing an interference frequency. The synthesized frequency IEMI signal can be expressed as:

$$s(t) = \sum_{m=1}^{M} A_m \cos\left(2\pi f_m t + \phi_m\right) \tag{6}$$

Where M is the number of interference frequency components, A_m is the amplitude of the m-th interference signal, f_m is the frequency of the m-th interference signal, and ϕ_m is the phase offset of the m-th interference signal. Fig. 4 presents the time-frequency representation of the synthesized frequency IEMI signal after down-converting to the baseband. The signal consists of three discrete frequency components within a 10 MHz bandwidth, originally centered at 2.16 GHz. These components are visible as distinct horizontal lines in the spectrogram, showing the consistency of the synthesized frequency content in the detection window of 500 μs.

E. Time-Series Feature Extraction

As demonstrated by the classification and modeling above, the features of EMI and IEMI in railway communications are time-varying, primarily due to the train's movement and the changing propagation environment. As the train progresses along a fixed route, the evolution of the received signal can be effectively captured and analyzed using deep learning techniques designed for time-series data. Existing research in the field primarily focuses on detecting and classifying signal types by analyzing frequency spectrum features. These studies

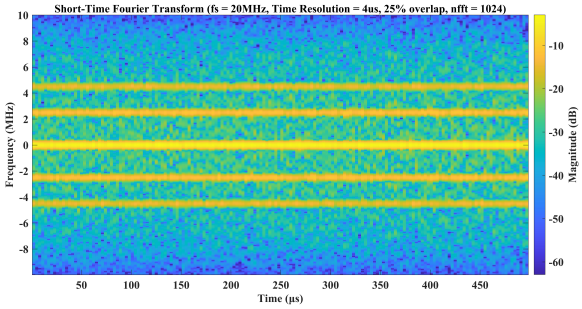

Fig. 4. Time-frequency representation of the synthesized frequency IEMI on the ground

compare the performance of various machine learning models by generating large datasets using these parameters. However, they tend to overlook that the type of interference depends on the time-series characteristics. Detecting and classifying interference without considering the variations in signal characteristics over time is fundamentally flawed, and often results in inaccurate results.

The time series feature extraction process from the received signals are shown in Fig. 5. The signal received by antenna is initially sampled at 6 GHz, and then down-converted to 20 MHz. The data is collected and analyzed based on this 20 MHz sampling frequency. The choice of 20 MHz sampling frequency is because the signal has a bandwidth of 10 MHz. In our previous research [36], sampling was performed directly at 6 GHz, which resulted in an overwhelming amount of data that was computationally expensive to process. Moreover, we could only detect a 100 μs time interval every second, which led to unreliable and non-robust detection and classification accuracy. By down-converting and using a lower sampling rate, we are able to achieve more efficient data processing and improve the reliability of detection and classification results.

The signal received from the antenna is inherently complex due to the use of in-phase (I) and quadrature (Q) components in I/Q sampling techniques. This method captures both the amplitude and phase information of the signal, which is essential for accurately characterizing complex-valued signals with overlapping frequency components as shown in [37]. In our analysis, the time-series data obtained from the STFT consists of 1024 features corresponding to the frequency bins of the transformed signal. We separate this complex data into its real part (I component) and imaginary part (Q component), effectively doubling the number of features. This results in a total of 2048 distinct time-series features. By including both the I and Q components, we preserve the signal's full amplitude and phase information, providing richer input for the deep learning model to capture intricate EMI and IEMI patterns, and improving classification performance in dynamic HSR environments.

III. Detection and Classification Algorithm

A. Long short-term memory (LSTM) basis

The LSTM network is an improved version of recurrent neural networks (RNNs) that addresses the vanishing and

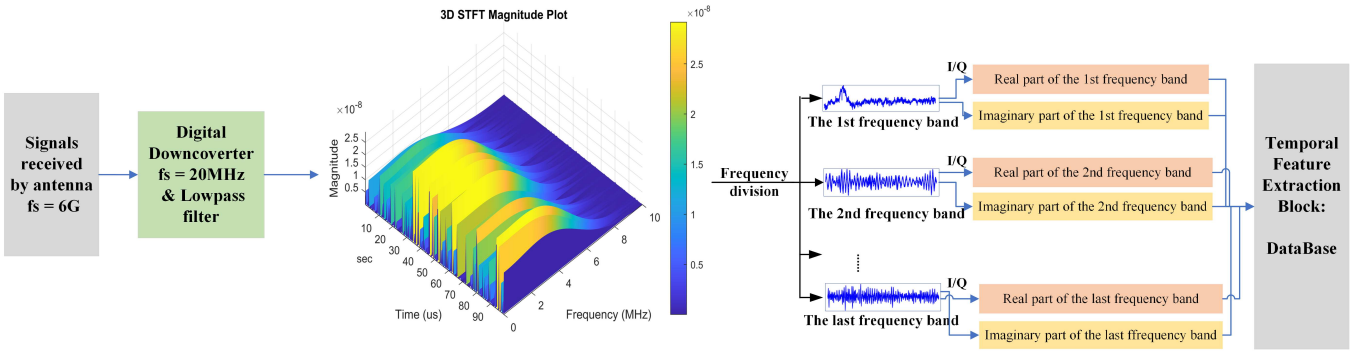

Fig. 5. Flowchart of the Time-Series Feature Extraction

exploding gradients issues [18], [19]. It achieves this by introducing forget gates, input gates, and output gates as shown in Fig. 6, which enhance the network's ability to remember important information and forget irrelevant information selectively.

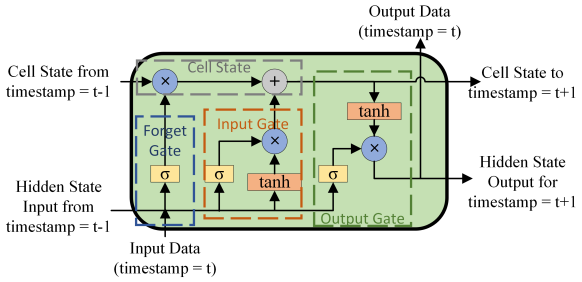

Fig. 6. Illustration of an LSTM cell [18]

Detecting signals in 5G-R can be challenging, especially when the carrier frequency is 2.16 GHz. In this study, a practical sampling frequency of 20 MHz is used to sample the received signal, which provides a balance between capturing the necessary information and managing computational complexity. The sampled data represents time-series data with a long duration, such as $\tau = 500\ \mu s$ in every $2ms$ time interval. Within the duration of the signal detection window, the algorithm must process this long time-series data effectively. Consequently, LSTM networks are introduced into the algorithm to capture features based on long-range temporal dependencies.

In addition to the LSTM network, a BiLSTM is employed to further improve the model's capability to capture dependencies in both forward and backward directions [7]. BiLSTM networks consist of two LSTM layers that process the input sequence in opposite directions, which allows the network to consider both past and future context for each time step. This characteristic is particularly useful for time-series data, where the relationships between data points are not solely dependent on the past but also on future inputs. Moreover, the data collected when the train is moving away from the BS can also be used to represent movement towards it, allowing for more comprehensive data training. By leveraging BiLSTM, the model can more effectively capture the dynamic nature of EMI and IEMI signals in high-mobility railway environments.

B. Attention mechanism basis

While LSTM networks are capable of capturing long-term dependencies in sequential data, they may still struggle with very long sequences due to limitations in retaining useful information over extended time steps. The forget gate in LSTM cells, although essential for mitigating the vanishing gradient problem, can sometimes lead to the loss of valuable information from earlier time steps. This can deteriorate the performance of the system when training on long sequences, e.g., our signal sequence is 166 timesteps within the duration of 500 μs. The attention mechanism addresses this issue by allowing the model to focus on specific parts of the input sequence, enhancing its ability to capture relevant information regardless of its position in the sequence.

Attention mechanisms in neural networks are inspired by the human visual system's ability to focus selectively on certain parts of the visual field to process information more efficiently. In the context of neural networks, attention allows models to dynamically assign different weights to different parts of the input data during training and inference. This technique has become popular in various applications, including natural language processing, image captioning, and time series analysis [20]. By integrating the attention mechanism into the BiLSTM network, the model can dynamically focus on specific parts of the input sequence by assigning adaptive weights to different temporal states, thereby improving accuracy and robustness. Existing works have shown that the combination of LSTM and attention mechanisms often results in superior performance in tasks involving sequential data, as it allows for more nuanced feature extraction and contextual understanding [23]–[25].

In our proposed model, the self-attention mechanism operates over the hidden states produced by the BiLSTM layers at each time step. These hidden states contain rich information about the input sequence, capturing features across 2048 channels as the result of the bidirectional processing. By applying self-attention to these hidden states, the model effectively captures dependencies between 166 time steps, allowing it

to focus on the most relevant parts of the sequence. In self-attention, the queries, keys, and values all originate from the same set of hidden states. This design enables the model to weigh the importance of each hidden state relative to others when computing a context vector ε. The context vector is a weighted sum of the hidden states, where the attention weights α_i reflect the importance of each hidden state in contributing to the final representation. The attention mechanism can be described in three steps, as illustrated in Fig. 7. The first step is to calculate the attention scores s_i which measure the relevance between the query and each key:

$$s_i = \tanh(Q \cdot K_i^\top), \tag{7}$$

herein, the dot method is used to compute the similarity. The keys K are derived from the hidden states and $K_i^\top$ is the transpose of the key vector at time step i. Queries Q represent the last moment derived from the hidden state. In the second step, the attention weights $\alpha = \{\alpha_1, \alpha_2, ...\alpha_t\}$ are obtained by applying the softmax function to the attention scores. This converts the scores into a probability distribution over the time steps:

$$\alpha_i = \frac{\exp(s_i)}{\sum_{j=1}^{t} \exp(s_j)}, \tag{8}$$

where α_i represents the importance of the hidden state at time step i. The third step is to calculate the context vector ε as the weighted sum of values:

$$\varepsilon = \sum_{i=1}^{t} \alpha_i V_i, \tag{9}$$

where values V are the same as the keys and are derived from the hidden states, and V_i is the value vector at time step i. By summing over all time steps with their respective attention weights, the context vector ε effectively captures the most relevant information from the entire sequence. This allows the model to focus on important features across different time steps, enhancing its ability to model long-range dependencies and improving overall performance.

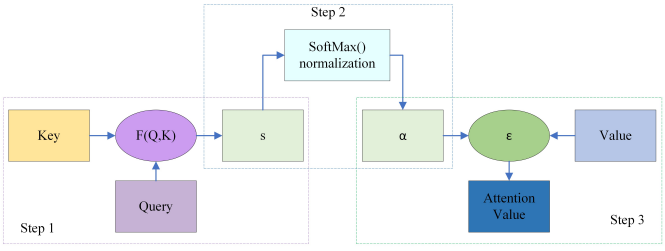

Fig. 7. Internal calculation process diagram of the attention mechanism [23]

C. Attention-BiLSTM-based Classification Algorithm

The structure of the proposed Attention-BiLSTM-based multiclass classification algorithm is depicted in Fig. 8. In this structure, the network is trained using the data collected under railway scenarios described in the previous session and their corresponding labels.

The EMI and IEMI detection approach proposed in this paper is designed to classify signals within a duration of τ of 500 μs. Given the time resolution of 4 μs and an overlap of 25%, 166-time steps are collected within the duration of 500 μs. In general, a longer detection window provides more accurate results as a result of the increase in the amount of data available for analysis, improving the robustness of signal classification. The choice of a 500 μs interval is made based on safety requirements, specifically the need to trigger an emergency brake in signal loss. The latency requirement for the emergency brake system is 10 ms [13], which means that any interference must be detected well in advance to allow sufficient time for an appropriate response. The $500\mu s$ window provides an optimal trade-off, ensuring accurate detection while minimizing the risk of latency-induced safety problems during train operations.

A stacked BiLSTM architecture is implemented to enhance the performance, each followed by a dropout layer. We observed that two BiLSTM layers provided the optimal balance between learning capacity and generalization performance. Models with more than two BiLSTM layers did not yield additional benefits and sometimes led to increased overfitting, while models with only one BiLSTM layer lacked sufficient capacity to model the intricate temporal relationships in the sequential data effectively. The dropout layers serve as a regularization mechanism, randomly deactivating the neurons with a rate during training to prevent overfitting [38].

The outputs of the forward and backward LSTM layers are then concatenated, creating an encoded representation $H_s = \{H_1, H_2, ..., H_t\}$. H_s, a feature vector with 2048 channels, combining both past and future information for each time step, is the input to the attention mechanism. By calculating the proportion of each moment in the time series to all moments, and further assigning different weight values to different time steps to get the context vector. H_t is a feature vector with 2048 channels derived from the last-moment hidden layer output. For the calculation of the context vector, H_t is compared with the time series hidden layer output H_s. Calculate the similarity between the H_s and H_t to obtain a weight vector α_t, and α_t is calculated with the time series hidden layer output H_s to obtain the context vector by weighted average, and then the context vector and the last moment hidden layer output H_t are spliced for further classification. The representation undergoes further processing in a fully connected layer for dimension reduction. The softmax activation function in the final layer transforms raw scores into a probability distribution across different classes, ensuring they sum up to 1. This probability distribution, denoted as Y_{ni}, is compared to the true label distribution T_{ni} using the cross-entropy loss formula presented in Fig. 8. The formula measures the dissimilarity, specifically the negative log-likelihood between the predicted and true class distributions. Here, N is the total number of classes, and C is an index representing a specific class, ranging from 1 to N, corresponding to the different classes: normal, transient EMI, onboard sweep IEMI, on-ground sweep IEMI, onboard synthesized IEMI, and on-ground synthesized IEMI.

During training, the algorithm iteratively adjusts its parameters (weights and biases) to minimize the cross-entropy

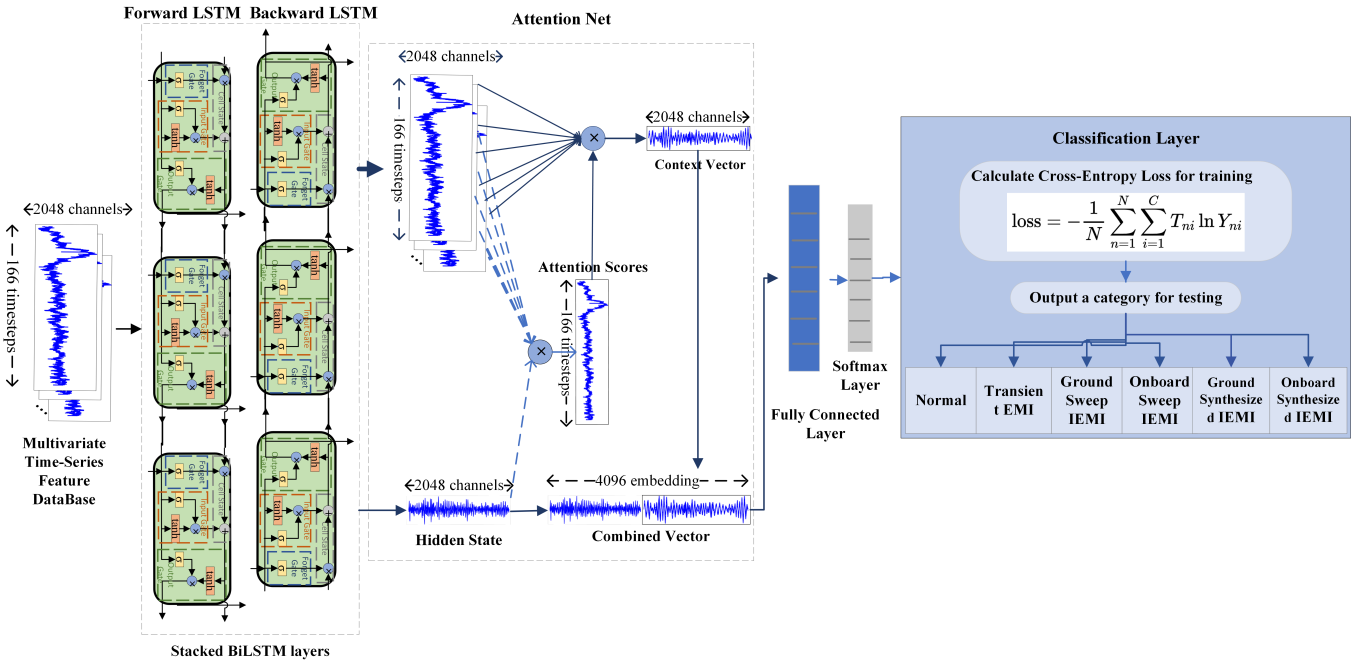

Fig. 8. Flowchart of Attention-BiLSTM-based Time Series Detection and Classification Algorithm

loss. This fine-tuning aims to enhance the model's ability to produce higher probabilities for the correct class and lower probabilities for other classes. During classification, the class with the highest probability in the output Y_{ni} is considered the predicted class. This decision is guided by the softmax function, which guarantees that the class with the highest raw score attains the highest probability.

By leveraging the Attention-BiLSTM framework, the proposed system benefits from both the temporal relationships captured by the bidirectional LSTM and the selective focus on critical time steps provided by the attention mechanism, which enhances the classification performance, even under complex high-mobility railway conditions.

IV. Simulation Results and Analysis

The railway wireless communication system model with Rician fading channel, Doppler shift, path loss, and ambient noise, provides a realistic platform for evaluating detection and classification systems under dynamic conditions. Data are collected as the train approaches and moves away from the BS with versatile speeds, within the coverage of one BS. The parameters of the simulation and analysis are listed in the TABLE I.

Five types of interferences are superimposed on the signals and collected within intervals containing multivariate time-series features. These data fall into six classes: normal conditions, transient EMI, onboard sweep IEMI, on-ground sweep IEMI, onboard synthesized IEMI, and on-ground synthesized IEMI. The simulations are conducted with a detection sampling interval of 500 μs every 2 ms, covering the distance ranging from the train to BS from 10 meters to a maximum of 1500 meters (assume the two consecutive 5G-R BSs are 3 km apart). In the simulation, five different train speeds (100, 200, 300, 400, and 500 km/h) and four different scenarios (Rural, Viaduct, Cutting, and Platform), defined by Rician channel fading K-factors and path loss exponents, are considered. The parameters of different scenarios are listed in TABLE II [39]–[42]. For each interference class at a specific scenario and speed, a total of 5,000 samples are collected. During the training phase, all six classes are included in the dataset, resulting in a total of 30,000 samples. The dataset is then divided into a training set of 70%, a validation set of 10%, and a test set of 20%.

TABLE I
Simulation Parameters

Parameter	Value
Distance from BS to rail	10 meters
Carrier Frequency	2.16 GHz
Detection Bandwidth	2155 to 2165 MHz
Detection Sampling Frequency	20 MHz
Train Movement Duration	10 s
Detection Sampling Interval	500 μs every 2 ms
Train Five Different Speed	100, 200, 300, 400, 500 km/h
Four Different Scenarios	Rural, Viaduct, Cutting, Platform
Ambient Noise Model	AWGN with SNR 20 dB
BS transmitted signal amplitude	1V
Output power jammer	1 W or +30 dBm
Deep learning optimizer	Adam
Initial learning Rate α	0.001
Gradient Threshold	1
Max-Epochs	100
Mini-Batch Size	200
Hidden Units of BiLSTM Layer	512, 128
Dropout Rate	0.3

The train speeds and channel conditions are varied to evaluate the robustness of the proposed classification approach in different railway environments. By learning these realistic operational conditions, the model is trained to effectively

classify the signals under diverse and challenging scenarios. The training process aims to optimize the model's ability to detect and classify interference types while maintaining reliability at high speeds and varying environments from the BS.

TABLE II
PARAMETERS FOR RAILWAY WIRELESS COMMUNICATION SCENARIOS

Scenario	Rician K Factor μ (dB), σ (dB)	Path Loss Exponent n	Doppler Shift (Hz) (up to 500 km/h)
Rural	$\mu = 6$, $\sigma = 3.5$	$2.0 \sim 2.5$	$0 \sim 1000$
Viaduct	$\mu = 4.16$, $\sigma = 3.94$	$2.5 \sim 4.0$	$0 \sim 1000$
Cutting	$\mu = 1.52$, $\sigma = 4.67$	$4.0 \sim 4.5$	$0 \sim 1000$
Platform	$\mu = 5$, $\sigma = 5.6$	$2.5 \sim 5.0$	$0 \sim 1000$

A. Performance Evaluation

1) Classification performance across various speeds and scenarios: To evaluate the proposed method, data from five different train speeds were collected and analyzed under rural scenarios. TABLE III shows the classification accuracy achieved for each interference type at different train speeds. The results show that normal conditions can be distinguished from interference signals more easily at lower speeds, and interference classes (transient EMI, sweep frequency, and synthesized frequency) can also be distinguished. Moreover, transient EMI can be easily detected as its short-term variation is more resolved, particularly at lower speeds. While at high speeds, transient EMI occurs more frequently, leading to missed detections. Onboard and on-ground interference tend to be mixed at lower speeds. In contrast, as the train moves further within the same detection duration at higher speeds, the channel effect and Doppler shift create observable differences between onboard and on-ground interference, enabling the deep learning network to detect and classify these interferences more effectively. However, the useful signal can also be more difficult to capture due to increased variations, leading to false alarm problems and a lower precision rate.

TABLE III
CLASSIFICATION ACCURACY ACHIEVED BY DIFFERENT TRAIN SPEEDS

Speed (km/h)	Normal	Transient EMI	Onboard Sweep IEMI	Ground Sweep IEMI	Onboard Synth. IEMI	Ground Synth. IEMI
100	100%	96.7%	100%	92.9%	94.4%	95.4%
200	99.6%	95.94%	98.38%	91.67%	95.88%	95.4%
300	98.6%	91.25%	96.52%	91.56%	96.48%	94.89%
400	98.24%	89.47%	95.06%	92.67%	96.95%	94.9%
500	98.24%	87.47%	94.06%	91.17%	96.85%	93.5%

Data from four different railway scenarios were collected and analyzed at a train speed of 300 km/h. TABLE IV shows the classification accuracy achieved for each interference type in different railway scenarios. The results indicate that interference signals are more easily detected in rural areas with a predominance of LOS paths and fewer reflections, followed by viaduct, cutting, and platform scenarios. The rural scenario, characterized by a higher K factor, stronger LOS components, and a lower path loss exponent, allows for clearer detection with minimal false alarms. Similarly, the viaduct scenario performs well, with a moderate K factor and path loss exponent. However, cuttings may introduce signal reflections and attenuation, impacting the reconstruction loss and reducing detection accuracy. The precision of detection is notably influenced by the dynamic propagation channel characteristics. The platform scenario is the most challenging due to crowding and numerous electronic devices, which contribute to significant on-ground interference, thereby increasing the level of IEMI. Additionally, the useful signals are harder to capture due to reflections from the station structures. Overall, the consistently high accuracy across all scenarios underscores the adaptability of the Attention-BiLSTM classification algorithm. This performance instills confidence in the system's suitability for diverse real-world railway deployment scenarios, demonstrating robustness across varying conditions.

TABLE IV
CLASSIFICATION ACCURACY ACHIEVED BY DIFFERENT TRAIN SPEEDS

Scenario	Normal	Transient EMI	Onboard Sweep IEMI	Ground Sweep IEMI	Onboard Synth. IEMI	Ground Synth. IEMI
Rural	98.6%	91.25%	96.52%	91.56%	96.48%	94.89%
Viaduct	97.6%	90.04%	94.38%	89.67%	94.4%	92.8%
Cutting	96.9%	89.25%	91.52%	89.56%	92.48%	92.4%
Platform	92.24%	85.47%	89.06%	87.67%	91.85%	91.4%

To further illustrate the effectiveness of the proposed method, we highlight some typical scenarios that are representative of different operational conditions. For example, a low-speed scenario (100 km/h) combined with the platform environment is useful for analyzing communication performance in station or platform areas. For high-speed conditions, such as 400-500 km/h combined with the rural scenario, the model's ability to handle a stable LOS path with fewer reflections can be evaluated. For medium-speed scenarios, such as 200-300 km/h combined with viaduct and cutting environments, the analysis focuses on communication in common train operational conditions, where moderate reflections and varying channel characteristics exist. Fig. 9 presents a bar chart comparing the average accuracy of interference classification across different train speeds for four distinct scenarios: Rural, Viaduct, Cutting, and Platform. The x-axis represents the five different train speeds (100, 200, 300, 400, and 500 km/h), while the y-axis shows the average classification accuracy. The results indicate that, for all scenarios, the classification accuracy tends to decrease with increasing train speed, which is likely due to the increased channel dynamics and higher Doppler effects at higher speeds. The Rural scenario consistently outperforms the other scenarios across all speeds, owing to its higher LOS component and fewer reflections, which contribute to a more stable propagation environment. The Viaduct scenario also demonstrates good performance, albeit slightly lower than Rural, due to moderate reflections and fewer obstacles compared to Cutting and Platform. The Cutting scenario shows a noticeable drop in accuracy at higher speeds, likely caused by the increased signal attenuation and reflections. The Platform scenario exhibits the lowest accuracy across all speeds, primarily because both onboard and trackside IEMI sources are located either within the train or very close to the train and coexist with a high density of electronic devices and complex structural reflections in a confined plat-

form environment, making it harder to distinguish their time-frequency signatures. Despite these challenges, the Attention-BiLSTM classification algorithm maintains relatively high accuracy, demonstrating its robustness and adaptability to diverse railway environments.

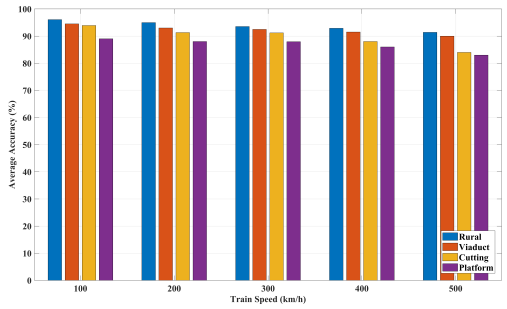

Fig. 9. Average Accuracy vs. Train Speeds for Different Scenarios

2) Ablation studies: To further understand the contribution of different components of the proposed model, ablation studies were conducted to evaluate the impact of removing key components: the Attention Mechanism and stacked BiLSTM layers. The following ablations were performed to assess the performance metrics, specifically focusing on classification accuracy and false alarm rate.

- Without Attention Mechanism: The attention layer was removed, and the results indicated a significant drop in accuracy. This demonstrates the role of attention in identifying important temporal dependencies in the signal.
- Without stacked BiLSTM: The network was reduced to a single BiLSTM layer to evaluate the effect of reducing the network's learning capacity. Accuracy was moderately impacted, while the false alarm rate increased slightly, suggesting that stacked BiLSTM layers help in capturing long-term dependencies more effectively. When there are more than two BiLSTM layers, the false alarm rate increases considerably, indicating overfitting issues.

TABLE V
ABLATION STUDY PERFORMANCE METRICS

Ablation Study	Classification Accuracy(%)	False Alarm Rate(%)	Offline Training Time(s)	Online Detection Time(ms)
BiLSTM (1-layers)	91.9	1.8	6105	6.80
BiLSTM (2-layers)	92.05	1.5	6295	6.98
BiLSTM (3-layers)	92.66	1.9	6410	7.05
BiLSTM (1-layers)+Attention	92.76	1.2	7304	7.10
BiLSTM (2-layers)+Attention	94.98	0.5	7360	7.43
BiLSTM (3-layers)+Attention	93.24	1.7	7464	7.51

TABLE V summarizes the performance metrics for each ablation study: the Attention Mechanism and stacked BiLSTM components play crucial roles in achieving high accuracy and maintaining a low false alarm rate. The simulation experiments are implemented by Matlab 2023b. The test platform consists of an Intel(R) Core(TM) i9-14900HX CPU at 2.20 GHz with 64.0 GB RAM and an NVIDIA GeForce RTX 4060 Laptop GPU. The offline training time and online detection time metrics highlight the trade-offs between model complexity and real-time performance. The online detection time is measured in milliseconds, while the training time is measured in seconds. Despite our model incurring longer training and online detection times than conventional machine learning methods [6], [9], [15], [35], it only takes 7.43 milliseconds to process the online detection, which falls within the tolerance of 3GPP critical data communications latency requirements of 10 ms [13]. The interval is established based on triggering the emergency brake in case of signal loss and considering the tolerance of signal variance during the movement of the train. Overall, the ablation studies emphasize the importance of each component in contributing to the robustness and reliability of the proposed classification algorithm. Our proposed Attention-BiLSTM method effectively responds to interference when real-time detection and classification are paramount.

3) Performance Comparison with State-of-the-Art Methods: To further evaluate the performance of the proposed model, we employed the Receiver Operating Characteristic (ROC) curve, which plots the true positive rate against the false positive rate at various classification thresholds. This provides a visual representation of the trade-off between sensitivity and specificity across different threshold values. A ROC curve that is closer to the top-left corner, indicating a larger area under the curve (AUC), signifies superior performance. Since ROC curves are originally designed for binary classification tasks, we adopted a one-vs-all strategy for our multiclass classification problem. In this approach, each class is individually treated as the positive class while the remaining classes are considered negative. This process was repeated for each of the six classes, and an average ROC curve was computed for each classification method.

The proposed Attention-BiLSTM model was compared with other common machine learning methods for multiclass classification, including BiLSTM without attention layer, SVM, RF, and AHC [9], [15], [18], [35], [36]. All models were trained and tested under the same conditions to assess their classification performance as illustrated in Fig. 10. The results demonstrate that the Attention-BiLSTM model outperforms BiLSTM, SVM, RF, and AHC. Specifically, the AUC value of the proposed Attention-BiLSTM algorithm was the highest, reaching 0.9956, which indicates superior detection and classification capabilities. The BiLSTM achieved the second-highest AUC value, followed by SVM, RF, and then AHC.

Overall, our proposed Attention-BiLSTM deep learning method effectively handles time-series data by analyzing both temporal and frequency characteristics simultaneously. This enables higher detection accuracy and adaptability in varying attenuation scenarios, making it particularly effective when real-time detection and classification are crucial. The results demonstrate that the Attention-BiLSTM model not only provides improved accuracy but also maintains robustness in different speeds and scenarios, underscoring its potential for real-world deployment.

V. REAL-DATA VALIDATION AND DISCUSSION

To further validate the practical applicability of the proposed methods, we conducted simulations using real-world

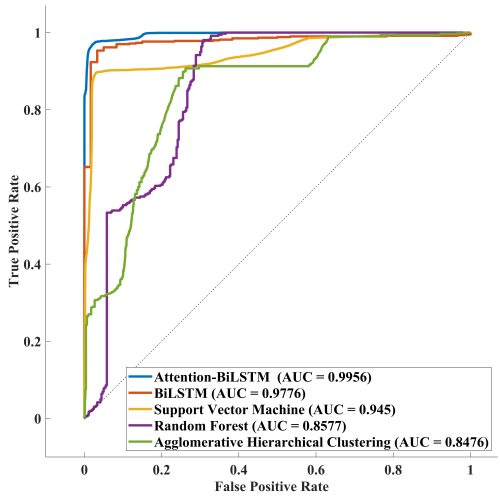

Fig. 10. ROC curves of multiclass-classification method comparison

channel data, which serves as a highlight of this paper. Since operational 5G-R lines carrying live EMI/IEMI signals are not yet available due to regulatory constraints, a fully real labeled interference dataset cannot be obtained. Therefore, we constructed a hybrid dataset by superimposing simulated EMI/IEMI waveforms onto real-channel recordings captured from the Beijing Jiaotong University 5G-R test line. The BS is placed 10 m away from the railway track, with an antenna height of 25 m. A two-carriage-length train moved along the track at a speed of 80 km/h. Receiver antennas were mounted on the roof of the train to maintain a clear LOS with the BS antenna.

The measurement system consists of the following components: signal transmitter and receiver, reference clock, antenna array and electronic switch, power supply equipment. The transmitter utilized a National Instruments (NI) PXIe-5673 vector signal generator to emit signals at a central frequency of 2.16 GHz within a 10 MHz bandwidth. An omnidirectional microstrip antenna was used to ensure uniform signal propagation in all directions. Two types of receivers were used as vector signal analyzers: Receiver 1: The NI USRP-2954; Receiver 2: The NI PXIe-5663, features a 16-element dual-polarized cylindrical antenna array, down-convert radio frequency signals to baseband and then stores them in a data disk. Table VI summarizes the configurations of the measurement system. More details of the measurement system can be found in [43]–[45].

TABLE VI
CONFIGURATIONS OF MEASUREMENT SYSTEM

Parameter	Value
Maximum transmit power (dBm)	40
Number of frequency points	513
Receiver 1 Sampling Rate	500 snapshots/s
Receiver 2 Sampling Rate	160 snapshots/s
Height of BS Antenna (m)	25
Height of Receiver Antenna (m)	3.5
Train Speed	80 km/h

We construct a simulated orthogonal frequency-division multiplexing (OFDM) downlink using binary phase-shift keying (BPSK) to capture the spectral characteristics. In the data collection process using the snapshot device, the receiver sampled the continuous signal at a rate of 20 MHz, corresponding to a time interval of 50 ns between each snapshot. Consequently, the total time for capturing one snapshot, representing one complete OFDM symbol, was $1024 \times 50\ ns = 51.2\ \mu s$. The acquisition of the signal spectrum relies on multiple snapshots within a 51.2 μs duration obtained by the antenna array, effectively capturing the complete information of all subcarriers of the OFDM symbol. Each snapshot records the signal received by each element of the antenna array, and these signals are subsequently used as features to train the deep learning model. To extract the frequency components corresponding to the 1,024 subcarriers, an STFT is applied to the sampled signal at the receiver. This transformation provides detailed amplitude and phase information for each subcarrier, which is crucial for analyzing the frequency-domain characteristics of the received signal, especially for short time-series analysis. In theory, the snapshot device can capture approximately 19,531 OFDM symbols per second, each containing a full 1,024 subcarrier information. However, due to practical hardware limitations, including processing speed, memory capacity, and data transfer rates, the number of snapshots that could be practically collected was reduced to 39 times and around 500 OFDM symbols per second [46], [47]. Consequently, the characteristics of the received signal were captured at intervals of approximately 2 ms. The total duration of the operation is 336 seconds and 334 seconds for the two receivers respectively, during which data was continuously collected as a matrix as 1024×166000 and $1024 \times 16 \times 5444$.

To train our neural network, we processed each OFDM symbol (1024 sub-carriers) to construct time-series inputs comprising 166-time steps within a detection window of 500 μs. Linear interpolation was employed between consecutive OFDM symbols to simulate temporal dynamics and create finer time steps. Specifically, the stored subcarriers were interpolated across 166 evenly spaced time points within each detection window, resulting in a matrix of features and timesteps as 1024×166. This approach allows the network to learn and model the signal's behavior over smaller intervals while respecting the hardware's constraints. The resulting time-series data were then fed into the network for training, allowing it to learn the temporal dependencies and patterns present in the signal over the specified interval.

The confusion matrix summarizes the performance of a classification algorithm by comparing its predictions with the actual class labels in a data set shown in Fig. 11. The performance of our multi-classification model shows that it can achieve a high accuracy of 92.5% on the hybrid test dataset containing 6,000 samples. Notably, the algorithm excels in distinguishing normal conditions and transient EMI across the classes with minimal errors. Misclassifications and misdetections primarily occur between onboard and on-ground IEMI classes, probably due to their similar characteristics at the relatively low speed of 80 km/h. Despite these challenges, the accuracy remains closely aligned with that of the purely sim-

ulated dataset (94.98%), confirming the model's robustness.

The hybrid dataset preserves realistic propagation effects, hardware impairments, and the noise of a real 5G-R environment while retaining access to accurately labeled interference classes. This validation approach effectively bridges the gap between pure simulations and the currently unavailable fully interfered field datasets, demonstrating the model's practical applicability in real-world railway wireless communication systems and its suitability for safety-critical EMI/IEMI detection and classification tasks.

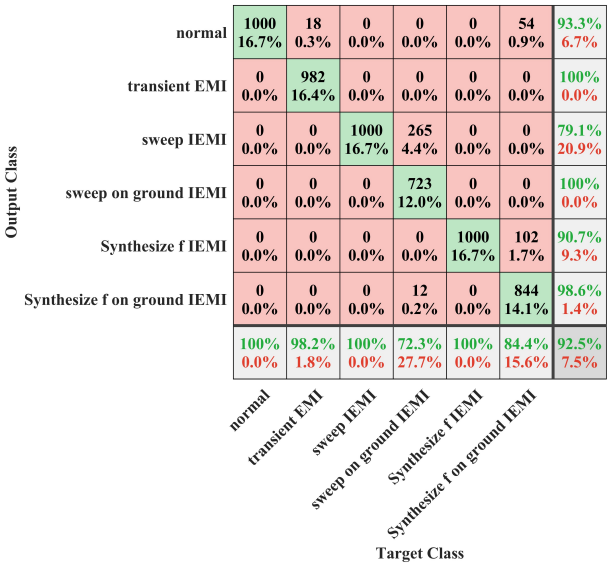

Fig. 11. Confusion matrix of the multi-classification model on real data test set

VI. Conclusion

In this paper, a comprehensive model for future intelligent high-mobility 5G-R is constructed, considering the dynamic channel model and potential EMI threats. The time-series signals are analyzed in both real and imaginary components, incorporating fine-resolution time and frequency information to capture the intricate characteristics of railway communication environment. The Attention-BiLSTM detection and classification algorithm is used to classify different types of EMI in a dynamic environment, utilizing stacked BiLSTM layers integrated with an attention mechanism. Simulations are conducted across four typical railway scenarios at train speeds up to 500 km/h. The result achieves a classification accuracy of 94.98%, improving by 3% compared to the state-of-the-art methods. Furthermore, it demonstrates online detection capabilities with a latency of 7.43 ms, meeting the 10 ms real-time safety requirements. Validation using real-world data with an accuracy of 92.5% proves its effectiveness in practical applications. Future work will focus on extending this classification framework by conducting experiments on operational 5G-R testbeds across diverse railway scenarios to generate a comprehensive labeled dataset. Based on the proposed real-time classification methods, further mitigation and signal resistance strategies can be developed to enhance resilience of railway wireless communications against EMI, laying a solid foundation for improving reliability of railway communication systems and contributing to advancement of intelligent transportation technologies.

References

[1] B. Ai, A. F. Molisch, M. Rupp, and Z.-D. Zhong, "5G key technologies for smart railways," *Proceedings of the IEEE*, vol. 108, no. 6, pp. 856–893, 2020.

[2] P. Fan, J. Zhao, and C.-L. I., "5G high mobility wireless communications: Challenges and solutions," *China Communications*, vol. 13, pp. 1–13, 01 2016.

[3] R. He, B. Ai, Z. Zhong, M. Yang, R. Chen, J. Ding, Z. Ma, G. Sun, and C. Liu, "5G for railways: Next generation railway dedicated communications," *IEEE Communications Magazine*, vol. 60, no. 12, pp. 130–136, 2022.

[4] 5GRail, "High-level concluding report 5GRAIL - the first FRMCS demonstrator the story, the outcome, what's next," 2024. [Online]. Available: https://5grail.eu/wp-content/uploads/2024/03/5GRAIL_Concluding_Report.pdf

[5] B. Ai, X. Cheng, T. Kürner, Z.-D. Zhong, K. Guan, R.-S. He, L. Xiong, D. W. Matolak, D. G. Michelson, and C. Briso-Rodriguez, "Challenges toward wireless communications for high-speed railway," *IEEE Transactions on Intelligent Transportation Systems*, vol. 15, no. 5, pp. 2143–2158, 2014.

[6] J. Villain, V. Deniau, and C. Gransart, *Jamming Detection in Electromagnetic Communication with Machine Learning: A Survey and Perspective*, ser. Machine Learning and Probabilistic Graphical Models for Decision Support Systems. CRC Press, 10 2022.

[7] Y. Fan, L. Zhang, and K. Li, "AE-BiLSTM: Multivariate time-series emi anomaly detection in 5G-R high-speed rail wireless communications," in *2024 IEEE International Conference on Communications Workshops (ICC Workshops)*, 2024, pp. 439–444.

[8] S. Soderi, D. Masti, and Y. Z. Lun, "Railway cyber-security in the era of interconnected systems: A survey," *IEEE Transactions on Intelligent Transportation Systems*, vol. 24, no. 7, pp. 6764–6779, 2023.

[9] J. Villain, V. Deniau, A. Fleury, E. P. Simon, C. Gransart, and R. Kousri, "EM monitoring and classification of IEMI and protocol-based attacks on ieee 802.11n communication networks," *IEEE Transactions on Electromagnetic Compatibility*, vol. 61, no. 6, pp. 1771–1781, 2019.

[10] Y. Fan, L. Zhang, and K. Li, "EMI and IEMI impacts on the radio communication network of electrified railway systems: A critical review," *IEEE Transactions on Vehicular Technology*, vol. 72, no. 8, pp. 10 409–10 424, 2023.

[11] H. Pirayesh and H. Zeng, "Jamming attacks and anti-jamming strategies in wireless networks: A comprehensive survey," *IEEE Communications Surveys & Tutorials*, vol. 24, no. 2, pp. 767–809, 2022.

[12] Z. Ma, X. Chen, M. Xiao, G. K. Karagiannidis, and P. Fan, "Interference control for railway wireless communication systems: Techniques, challenges, and trends," *IEEE Vehicular Technology Magazine*, vol. 15, no. 3, pp. 51–58, 2020.

[13] Ericsson, "White paper on 5G-powered future railway mobile communication system (FRMCS)," www.ericsson.com, 2022. [Online]. Available: https://www.ericsson.com/en/reports-and-papers/white-papers/5g-powered-frmcs

[14] A. Marttinen, A. M. Wyglinski, and R. Jäntti, "Statistics-based jamming detection algorithm for jamming attacks against tactical manets," in *2014 IEEE Military Communications Conference*, 2014, pp. 501–506.

[15] Y. Arjoune, F. Salahdine, M. S. Islam, E. Ghribi, and N. Kaabouch, "A novel jamming attacks detection approach based on machine learning for wireless communication," in *2020 International Conference on Information Networking (ICOIN)*, 2020, pp. 459–464.

[16] J. Villain, V. Deniau, C. Gransart, A. Fleury, and E. P. Simon, "Characterization of ieee 802.11 communications and detection of low-power jamming attacks in noncontrolled environment based on a clustering study," *IEEE Systems Journal*, vol. 16, no. 1, pp. 683–692, 2022.

[17] R. He and B. Ai, *Wireless Channel Measurement and Modeling in Mobile Communication Scenario*. CRC Press, 02 2024.

[18] H. Liu, H. Zhao, J. Wang, S. Yuan, and W. Feng, "LSTM-GAN-AE: A promising approach for fault diagnosis in machine health monitoring," *IEEE Transactions on Instrumentation and Measurement*, vol. 71, pp. 1–13, 2022.

[19] T. Zhou, H. Zhang, B. Ai, and L. Liu, "Weighted score fusion based lstm model for high-speed railway propagation scenario identification," *IEEE Transactions on Intelligent Transportation Systems*, vol. 23, no. 12, pp. 23 668–23 679, 2022.

[20] A. Vaswani, N. Shazeer, N. Parmar, J. Uszkoreit, L. Jones, A. N. Gomez, L. Kaiser, and I. Polosukhin, "Attention is all you need," in *Proceedings of the 31st International Conference on Neural Information Processing Systems*, ser. NIPS'17. Red Hook, NY, USA: Curran Associates Inc., 2017, p. 6000–6010.

[21] Y. Wang, X. Cai, X. Tang, S. Pan, Y. Wang, H. Yan, Y. Ren, and Y. Hou, "HSRA-Net: Intelligent Detection Network of Anomaly Monitoring Data in High-Speed Railway," *IEEE Transactions on Intelligent Transportation Systems*, vol. 25, no. 12, pp. 20 793–20 803, 2024.

[22] B. Liu, J. Chen, R. Wang, J. Huang, Y. Luo, and J. Wei, "Optimizing News Text Classification with Bi-LSTM and Attention Mechanism for Efficient Data Processing," in *2024 5th International Conference on Intelligent Computing and Human-Computer Interaction (ICHCI)*, 2024, pp. 281–285.

[23] M. Cao, R. Yao, J. Xia, K. Jia, and H. Wang, "LSTM Attention Neural-Network-Based Signal Detection for Hybrid Modulated Faster-Than-Nyquist Optical Wireless Communications," *Sensors*, vol. 22, no. 22, 2022.

[24] L. Mo, Y. Wang, W. Zhou, X. Shen, and W. Kong, "A Bi-LSTM Based Network with Attention Mechanism for EEG Visual Classification," in *2021 IEEE International Conference on Unmanned Systems (ICUS)*, 2021, pp. 858–863.

[25] J. Zhang, K. Li, B. Yang, and X. Han, "Local and global convolutional transformer-based motor imagery EEG classification," *Frontiers in Neuroscience*, vol. 17, 2023.

[26] L. Xiaoyan and R. C. Raga, "BiLSTM model with Attention mechanism for sentiment classification on chinese mixed text comments," *IEEE Access*, vol. 11, pp. 26 199–26 210, 2023.

[27] Y. Liang, H. Li, Y. Li, and A. Li, "Mainline Railway Modeled with 2100 MHz 5G-R Channel Based on Measured Data of Test Line of Loop Railway," *Symmetry*, vol. 16, no. 4, p. 431, Apr. 2024.

[28] R. He, B. Ai, Z. Zhong, M. Yang, C. Huang, R. Chen, J. Ding, H. Mi, Z. Ma, G. Sun, and C. Liu, "Radio communication scenarios in 5G-Railways," *China Communications*, vol. 20, no. 9, pp. 235–246, 2023.

[29] M. Heddebaut, V. Deniau, J. Rioult, and C. Gransart, "Mitigation techniques to reduce the vulnerability of railway signaling to radiated Intentional EMI emitted from a train," *IEEE Transactions on Electromagnetic Compatibility*, vol. 59, pp. 845–852, 06 2017.

[30] D. Mansson, R. Thottappillil, M. Backstrom, and O. Lunden, "Vulnerability of European rail traffic management system to radiated Intentional EMI," *IEEE Transactions on Electromagnetic Compatibility*, vol. 50, pp. 101–109, 02 2008.

[31] G. Matz, D. Schafhuber, K. Grochenig, M. Hartmann, and F. Hlawatsch, "Analysis, optimization, and implementation of low-interference wireless multicarrier systems," *IEEE Transactions on Wireless Communications*, vol. 6, no. 5, pp. 1921–1931, 2007.

[32] J. Oyarzun, I. Aizpuru, and I. Baraia-Etxaburu, "Time–frequency analysis of experimental measurements for the determination of emi noise generators in power converters," *Electronics*, vol. 11, no. 23, 2022.

[33] H. I. Ashqar, M. H. Almannaa, M. Elhenawy, H. A. Rakha, and L. House, "Smartphone transportation mode recognition using a hierarchical machine learning classifier and pooled features from time and frequency domains," *IEEE Transactions on Intelligent Transportation Systems*, vol. 20, no. 1, pp. 244–252, 2019.

[34] W. Radasky, C. Baum, and M. Wik, "Introduction to the special issue on high-power electromagnetics (HPEM) and intentional electromagnetic interference (IEMI)," *IEEE Transactions on Electromagnetic Compatibility*, vol. 46, no. 3, pp. 314–321, 2004.

[35] J. Villain, V. Deniau, E. P. Simon, C. Gransart, A. N. de São José, F. Valenti, and N. Becuwe, "Detection and classification of interference affecting lorawan communications in railway environment," in *2022 3rd URSI Atlantic and Asia Pacific Radio Science Meeting*, 2022, pp. 1–4.

[36] Y. Fan, L. Zhang, K. Li, M. Bao, and M. Lu, "Deep Learning-based EMI and IEMI Classification in 5G-R High-Speed Rail Wireless Communications," in *2024 IEEE 99th Vehicular Technology Conference (VTC2024-Spring)*, 2024, pp. 1–6.

[37] M. Naseri, E. De Poorter, I. Moerman, H. Vincent Poor, and A. Shahid, "High-throughput adaptive co-channel interference cancellation for edge devices using depthwise separable convolutions, quantization, and pruning," *IEEE Open Journal of the Communications Society*, vol. 6, pp. 656–670, 2025.

[38] M. Bao, M. Wang, K. Li, and X. Jia, "Integrating machine learning with sensor technology for multiphase flow measurement: A review," *IEEE Sensors Journal*, vol. 24, no. 19, pp. 29 603–29 618, 2024.

[39] R. He, Z. Zhong, B. Ai, G. Wang, J. Ding, and A. F. Molisch, "Measurements and analysis of propagation channels in high-speed railway viaducts," *IEEE Transactions on Wireless Communications*, vol. 12, no. 2, pp. 794–805, 2013.

[40] C.-X. Wang, A. Ghazal, B. Ai, Y. Liu, and P. Fan, "Channel measurements and models for high-speed train communication systems: A survey," *IEEE Communications Surveys Tutorials*, vol. 18, no. 2, pp. 974–987, 2016.

[41] B. Ai, R. He, Z. Zhong, K. Guan, B. Chen, P. Liu, and Y. Li, "Radio wave propagation scene partitioning for high-speed rails," *International Journal of Antennas and Propagation*, p. 815232, 01 2012.

[42] R. He, Z. Zhong, B. Ai, J. Ding, Y. Yang, and A. F. Molisch, "Short-term fading behavior in high-speed railway cutting scenario: Measurements, analysis, and statistical models," *IEEE Transactions on Antennas and Propagation*, vol. 61, no. 4, pp. 2209–2222, 2013.

[43] X. Zhang, R. He, M. Yang, S. Gao, Z. Qi, Z. Zhang, B. Ai, and Z. Zhong, "Measurement-based channel characterization and modeling for 5G-Railways at 2.16 GHz," in *2024 16th International Conference on Wireless Communications and Signal Processing (WCSP)*, 2024, pp. 254–259.

[44] M. Yang, B. Ai, R. He, C. Huang, Z. Ma, Z. Zhong, J. Wang, L. Pei, Y. Li, and J. Li, "Machine-Learning-Based Fast Angle-of-Arrival Recognition for Vehicular Communications," *IEEE Transactions on Vehicular Technology*, vol. 70, no. 2, pp. 1592–1605, 2021.

[45] X. Zhang, R. He, M. Yang, J. Ding, R. Chen, S. Gao, Z. Qi, Z. Zhang, B. Ai, and Z. Zhong, "Measurement-based nonstationary markov tapped delay line channel model for 5G-Railways," *IEEE Antennas and Wireless Propagation Letters*, vol. 24, no. 8, pp. 2277–2281, 2025.

[46] X. Zhang, R. He, M. Yang, Z. Qi, Z. Zhang, B. Ai, and R. Chen, "Narrowband Channel Measurements and Statistical Characterization in Subway Tunnels at 1.8 and 5.8 GHz," *IEEE Transactions on Vehicular Technology*, vol. 73, no. 7, pp. 10 228–10 240, 2024.

[47] X. Zhang, R. He, M. Yang, B. Ai, S. Wang, W. Li, W. Sun, L. Li, P. Huang, and Y. Xue, "Measurements and Modeling of Large-Scale Channel Characteristics in Subway Tunnels at 1.8 and 5.8 GHz," *IEEE Antennas and Wireless Propagation Letters*, vol. 22, no. 3, pp. 561–565, 2023.

VII. Biography Section

Yejing Fan is currently pursuing a Ph.D. degree in Electronic and Electrical Engineering at the University of Leeds, Leeds, U.K. She received a B.Eng. degree (First Class Honours) in Electrical and Electronic Engineering from both the University of Leeds, U.K., and Southwest Jiaotong University, Chengdu, China, in 2021. Her research interests include wireless communications, deep learning-based signal processing techniques, and electromagnetic interference (EMI) and intentional EMI (IEMI) issues in high-speed rail communication systems. In 2021, she was awarded the IEEE Prize for the best final-year undergraduate project in telecommunications.

Li Zhang (Senior Member, IEEE) is an Associate Professor in Communications at the School of Electronic and Electrical Engineering, University of Leeds. She leads the Wireless Communication Group within the Institute of Communication and Power Networks (ICaPNet). Her research focuses on wireless communications, including massive MIMO, mmWave and THz communications, Non-Terrestrial Networks (NTNs), mobile edge computing and 5G/6G systems. Her group is also actively investigating wireless communication challenges in high-speed railway systems. She has served on the Technical Programme Committees of most major IEEE communications conferences since 2006 and is currently an associate editor for several IEEE journals. She has been a member of the UK EPSRC Peer Review College since 2006 and has served on grant review panels for both EPSRC and Royal Society. She also regularly reviews grant proposals for international funding bodies, including the Qatar National Research Fund, and agencies in Denmark and France, as well as book proposals for various academic publishers. She has acted as a PhD examiner for numerous universities within and outside the UK and has served as an external examiner for MSc programmes at other UK institutions. She received a Nuffield Award for newly appointed lecturers in 2005, became a Fellow of the Higher Education Academy in 2006, and was elevated to IEEE Senior Member in 2012.

Kang Li (Senior Member, IEEE) received the B.Sc. degree in industrial automation from Xiangtan University, Hunan, China, in 1989, the M.Sc. degree in control theory and applications from the Harbin Institute of Technology, Harbin, China, in 1992, the Ph.D. degree in control theory and applications from Shanghai Jiaotong University, Shanghai, China, in 1995, and the D.Sc. degree in engineering from Queen's University Belfast, Belfast, U.K., in 2015.

He currently holds the Chair of Smart Energy Systems with the University of Leeds, Leeds, U.K. From 1995 to 2002, he was with Shanghai Jiaotong University, the Delft University of Technology, and the Queen's University Belfast as a Research Fellow. From 2002 to 2018, he was a Lecturer in 2002, a Senior Lecturer in 2007, a Reader in 2009, and a Chair Professor in 2011 with the School of Electronics, Electrical Engineering and Computer Science, Queen's University Belfast. His research interests include nonlinear system modeling, identification, and control, and artificial intelligence, with applications to energy and power systems, smart grids, electric vehicles, electrification of railway systems, and energy management in energy-intensive manufacturing processes.

Mi Yang (Member, IEEE) received the M.S. and Ph.D. degrees from Beijing Jiaotong University, Beijing, China, in 2017 and 2021, respectively. He is currently an Associate Professor with the School of Electronics and Information Engineering, Beijing Jiaotong University. His research interests include wireless channel measurement and modeling, vehicular and railway communications, and AI in channel research.

Xuejian Zhang received the B.S. degree in communication engineering from Lanzhou Jiaotong University, Lanzhou, China, in 2021. He is currently pursuing the Ph.D degree with School of Electronic Information Engineering, Beijing Jiaotong University, Beijing, China. His research interests include wireless channel measurement and modeling, railway and vehicular communications and vision-aided channel prediction.

Ruisi He (Senior Member, IEEE) received the B.E. and Ph.D. degrees from Beijing Jiaotong University (BJTU), Beijing, China, in 2009 and 2015, respectively. He is currently a Professor with the School of Electronics and Information Engineering, BJTU. Dr. He has been a Visiting Scholar in Georgia Institute of Technology, USA, University of Southern California, USA, and Université Catholique de Louvain, Belgium. His research interests include wireless propagation channels, 5G and 6G communications. He has authored/co-authored 8 books, 5 book chapters, more than 200 journal and conference papers, as well as several patents. Dr. He has been an Editor of the *IEEE Transactions on Communications*, the *IEEE Transactions on Wireless Communications*, the *IEEE Transactions on Antennas and Propagation*, the *IEEE Antennas and Propagation Magazine*, the *IEEE Communications Letters*, the *IEEE Open Journal of Vehicular Technology*, and a Lead Guest Editor of the *IEEE Journal on Selected Area in Communications* and the *IEEE Transactions on Antennas and Propagation*. He served as the Early Career Representative (ECR) of Commission C, International Union of Radio Science (URSI). He received the URSI Issac Koga Gold Medal in 2021, the IEEE ComSoc Asia-Pacific Outstanding Young Researcher Award in 2019, the URSI Young Scientist Award in 2015, and several Best Paper Awards in IEEE journals and conferences.

Mowei Lu is currently working toward the Ph.D. degree at the University of Cambridge, Cambridge, U.K. Prior to that, he received the M.Phil. degree in engineering from the University of Cambridge, Cambridge, U.K in 2022, the B.Eng. degree in electronic and electrical engineering from Southwest Jiaotong University, Chengdu, China, and the B.Eng. (First Class) degree in electrical and electronic engineering from the University of Leeds, Leeds, U.K., both in 2021. In 2025, he was a Controls Engineer Intern with Tesla, Freiburg, Germany. His research interests include power quality control, flexible ac transmission systems, the application of wide-bandgap devices, and grid-forming converters. Mr. Lu was the recipient of Jardine Scholarship, Cambridge Trust International Scholarship, and IEEE PELS John G. Kassakian Fellowship.